

# Impact of bond-order loss on surface and nanosolid magnetism

W.H. Zhong<sup>a</sup>, Chang Q. Sun<sup>a,\*</sup>, S. Li<sup>b</sup>, H.L. Bai<sup>c</sup>, E.Y. Jiang<sup>c</sup>

<sup>a</sup> School of Electrical and Electronic Engineering, Nanyang Technological University, Nanyang Avenue, Singapore 639798, Singapore

<sup>b</sup> School of Materials Science and Engineering, The University of New South Wales, Sydney NSW2052, Australia

<sup>c</sup> Institute of Advanced Materials Physics and Faculty of Science, Tianjin University, Tianjin 300071, P.R. China

Received 11 October 2004; received in revised form 15 March 2005; accepted 22 March 2005

Available online 21 April 2005

## Abstract

Incorporating the recent bond-order-length-strength correlation mechanism [Sun CQ, Bai HL, Li S, Tay BK, Jiang EY, Acta Mater 2004;52:501] into the Ising convention and the Brillouin function has enabled the unusual magnetic behavior of a ferromagnetic nanosolid and a surface to be reproduced using Monte Carlo simulations. Examination of the size and temperature dependence of the saturation magnetization ( $M_S$ ) of a solid of various structures reveals that: (i) at low temperatures, the  $M_S$  increases inversely with solid size due to the contribution from the localized charges that are trapped by the deepened potential well of the lower-coordinated atoms in the surface skins; (ii) at the ambient temperatures, the  $M_S$  drops with solid size because of the bond-order loss that suppresses the Curie temperature of the specimen; (iii) the quantized features of the surface to volume ratio of the solid is responsible for the observed  $M_S$  oscillations of smaller clusters at low temperatures.

© 2005 Acta Materialia Inc. Published by Elsevier Ltd. All rights reserved.

**Keywords:** Nanostructures; Magnetism; Thermal stability

## 1. Introduction

The magnetism of a ferromagnetic surface and a ferromagnetic nanosolid has attracted tremendous interest because of their potential applications in areas such as high-density data storage [1], sensors [2] and bioprocessing [3] and their significance in fundamental science [4]. When the solid size is reduced to nanometer scale, the magnetic properties change with solid size. For example, the Curie temperature ( $T_C$ ) drops [5–7] and the coercivity ( $H_C$ ) increases, for a solid made of nanograins [8–10]; whereas for a free standing nanosolid, the  $H_C$  drops. Generally, the saturation magnetization ( $M_S$ ) increases with quantized features at low temperatures whereas the  $M_S$  drops at ambient temperatures when the solid size is reduced [11–15].

In the case of thin films, the magnetic moment ( $\mu$ ) of the atom in the surface region is larger than the corresponding  $\mu$  in the bulk [16,17]. For instance, compared to the bcc Fe bulk moment of  $2.2 \mu_B$ , the  $\mu$  for a surface Fe atom has been found theoretically to be enhanced: (i) by 15% to  $2.54 \mu_B$  for one monolayer (ML) Fe on 5 ML W(1 1 0) and (ii) by 29% to  $2.84 \mu_B$  for 2 ML Fe on 5 ML W(1 1 0) surface. The significant surface relaxation (–12%) of Fe(3 1 0) and Ni(2 1 0) [18] surfaces has also been found to enhance the atomic  $\mu$  by up to 27%. The  $\mu_B$  is the Bohr magneton.

The stronger surface effects should be significant in nanosolids since a large portion of atoms of the system is located at the curved surfaces. However, controversy remains in the measured size dependence of the magnetization,  $M_S(K_j)$ , of a ferromagnetic nanosolid with radius  $R_j$  [11–15]. For convenience, we use the dimensionless form of size  $K_j = R_j/d$ , where  $d$  is the diameter of an atom in the bulk. The  $M_S(K_j)$  of clusters was measured to increase inversely with the solid size at low  $T$  [19,20]. The

\* Corresponding author. Tel.: +65 6790 4517; fax: +65 6792 0415.

E-mail address: [ecqsun@ntu.edu.sg](mailto:ecqsun@ntu.edu.sg) (C.Q. Sun).

URL: <http://www.ntu.edu.sg/home/ecqsun/> (C.Q. Sun).

$\mu$  per atom of Fe, Co, and Ni (at 78–120 K) increases until the value of a free atom when the solid size is reduced to a cluster that contains 30 atoms or less; as the size is increased up to 700 atoms, the magnetic moments approach to the bulk limits [21]. The  $M_S$  of a 1.8 nm sized Co particle is about 30% higher than that of the bulk [21]. A cobalt surface atom carries a moment of  $2.28 \mu_B$  compared to the bulk value of  $1.73 \mu_B$  [22]. The  $M_S$  of Fe–Ni alloy films in the temperature range of 77–570 K increases gradually when the thickness is decreased from 75 to 35 nm [23]. In a Stern–Gerlach experiment conducted at  $\sim 22$  K, Cox et al. [19] found that the  $M_S$  of the freestanding iron nanoclusters containing 2–17 atoms to be larger than that of the bulk iron counterpart. Calculations using the tight binding approximation [24] suggested that the magnetic enhancement of Fe, Co and Ni atoms arise from atomic coordination number (CN) imperfection. However, in the same kind of Stern–Gerlach deflections, Heer et al. [11] measured that the atomic  $\mu$  for small iron clusters (50–230 atoms) drops with the number of atoms when the molecular beam nozzle temperatures are at around 300 K. This trend is similar to those observed at ambient temperature of Co [15] Pd<sub>96</sub>Fe<sub>4</sub> [12,13] Pd<sub>97.1</sub>Fe<sub>2.9</sub> [13], NiFe<sub>2</sub>O<sub>4</sub> [25,26] and Ni<sub>3</sub>Fe [14] alloy particles. Similarly, a remarkable reduction of the magnetization for Fe–Ni invar alloy (<40 nm) [27] and Ni thin films has been observed at room temperature [5,28]. The  $M_S$  for Fe<sub>3</sub>O<sub>4</sub> thin films [29] drops rapidly when the film thickness decreases from 70 nm. Small Pd<sub>100-x</sub>Fe<sub>x</sub> grains with  $x = 4, 6, 8, 12$  and a radius of approximately 5 nm at 4.2, 100 and 295 K show a typical superparamagnetic features with  $M_S$  values that are substantially smaller than those observed for the bulk [12]. Monte Carlo (MC) simulations of the dynamic behavior of the magnetic spin systems show inconsistent trends at different temperatures. For instance, in the mid temperatures, the  $M_S(K_j)$  drops with size [30–33], whereas, at low temperatures,  $M_S$  is enhanced when the solid size is reduced [34]. It appeared that the observations are conflicting if one ignores the temperature of measurement.

A number of outstanding theories have been developed to explain the unusual behavior of ferromagnetic nanosolids. The  $M_S$  suppression was explained [35] as the surface spins that are weakly coupled and more disordered in comparison to the strongly coupled bulk spins. The magnetization of the entire solid is then dominated by the interior spins that drop in number with the solid size. Alternatively, the  $M_S$  suppression at room temperature was explained as a result of the  $T_C$  suppression of the surface. The surface layer [15] is easily magnetically molten, which contributes little to the total magnetic momentum of the system [36].

Several shell structural models have been developed for the size enhanced magnetization [21,37] and suggested that the magnetic moment of individual atom is determined by its atomic CN [37]. By assuming bulk-like struc-

tures (such as fcc and bcc) and different global shapes (cube, octahedron and cube octahedron), the average magnetic moment were found to oscillate with the cluster size, coinciding with observations. Therefore, the magnetic “shell structure” reflects the progressive formation of concentric atomic layers [40]. The magnetic properties of transition metals have been described, as a first order approximation, using a simple rectangular d-band approximation [38] together with the second moment approximation [39]. It was assumed that the d-band splitting between the major and the minor spin caused by the exchange interaction is invariant for the cluster to the bulk solid, leads to the following empirical expression [40]:

$$\mu_i/\mu_b = \begin{cases} \mu_{\text{dim}}/\mu_b & \text{if } z_i \leq z_b(\mu_b/\mu_{\text{dim}})^2, \\ (z_b/z_i)^{1/2} & \text{otherwise,} \end{cases} \quad (1)$$

where  $\mu_b$  and  $\mu_{\text{dim}}$  are the magnetic moments of a bulk atom and of a dimer atom, respectively [39]. Subscript  $i$  denotes the atom in the  $i$ th atomic layer. In the case of Fe,  $\mu_b = 2.22 \mu_B$  [41] and  $\mu_{\text{dim}} = 3.2 \mu_B$  [42]. For  $z_b = 12$ , the step function transits at  $z_i \sim 6$ . That is, an atom will take the  $\mu_{\text{dim}}$  value if its CN is six or less.

A model is highly desirable to reconcile the size and temperature dependence of  $M_S(K_j, T)$  and the  $M_S(K_j \sim 0, T \sim 0)$  oscillation in experimental and theoretical observations. Here, we show that incorporating the recent bond-order-length-strength (BOLS) correlation mechanism [43–45] to the Ising model could reproduce all the observed trends using MC calculations and hence reconcile the discrepancy in the unusual magnetic behavior of a ferromagnetic nanosolid of different shapes and crystal structures at different temperatures.

## 2. Principle

### 2.1. Ising model

The Hamiltonian of an Ising spin system in an external field is expressed as:

$$H = \sum_{\langle i,j \rangle} J_{\text{exc}} S'_i S'_j - g_J \mu_B B \sum_{i=1}^N S'_i, \quad (2)$$

where  $\langle i, j \rangle$  denotes a pair of nearest neighbors and  $S'_i$  is the atomic magnetic spinner which takes the total angular momentum,  $J_i$ , of the specific atom at site  $i$ .  $J_{\text{exc}} \propto r_{ij}^{-1}$  is the exchange strength,  $g_J$  is the Landé's  $g$ -factor, and  $B$  is the applied magnetic field.

### 2.2. BOLS derivation

#### 2.2.1. Surface magnetic moment

The BOLS correlation mechanism [46,47] indicates that the CN imperfection of an atom at a surface or at site surrounding defect causes the remaining bonds of

the lower-coordinated atom to contract to  $d_i = c_i d$  with  $c_i$  coefficient [46], spontaneously, associated with bond strength gain, or potential well depression, to  $E_i = c_i^{-m} E_b$ .  $E_i$  and  $E_b$  is the cohesive energy per bond of an atom in the  $i$ th atomic shell and in the bulk, respectively. The power index  $m$  is an indicator for the bond nature. As such, energy densification happens in the surface skin whereas the atomic cohesive energy ( $E_{B,i} = z_i E_i$ ) is weakened despite the bond strength gain, as illustrated in ([47], Fig. 2). Meanwhile, charge localization due to potential well depression contributes to the  $J_i$  of the lower-coordinated atom. If the localization probability is proportional to the well depth, then the densely localized electrons contribute to the  $J_i$  in such a way:

$$\begin{cases} \frac{J_i(z_i)}{J_b} \propto \frac{\mu_i(z_i)}{\mu_b} \propto \frac{E_i}{E_b} = c_i^{-m}, \\ c_i = 2/[1 + \exp((12 - z_i)/(8z_i))]. \end{cases} \quad (3)$$

The effective magnetic momentum along the applied field direction of a  $z_i$  coordinated atom is  $\mu_{iz} = J g_J \mu_B$ . Note that the lande’s  $g$ -factor ( $g_J = 1-2$ ) is a function of the orbital ( $L$ ) and spin ( $S_p$ ) angular momentum:  $g_J = 1 + [J(J + 1) + S_p(S_p + 1) - L(L + 1)]/[2J(J + 1)]$ , which is also affected by the CN imperfection. However, in the first order approximation, we neglect this effect that may influence the precision of  $m$  parameterization. As such, for an atom at a flat surface with  $z_i = 4$  ( $c_1 = 0.88$ ), the  $\mu_i$  increases by  $0.88^{-1} = 12\%$ , which is close to the cases of Fe–W, Fe–Fe and Ni–Ni of which the interlayer distance contracts by 10–12% associated with 15–29% enhancement of the  $\mu_i$  [48]. For a dimer,  $z_i = 2$ ,  $c_i = 0.7$ , the  $\mu_i$  is enhanced by 40%, agreeing with reported value of  $3.2/2.22$ , for Fe instance. By taking the effect of atomic CN imperfection and the pronounced portion of surface atoms into consideration, the magnetic properties of the ferromagnetic nanosolids should differ from those of the bulk.

### 2.2.2. Brillouin function

It is often to use the concept of “molecular field” to approximate the spontaneous magnetization at  $T$  in terms of Brillouin function,  $B_J(y)$  for a bulk [49]:

$$M(T) = g_J J \mu_B B_J(y),$$

$$B_J(y) = \frac{2J + 1}{2J} \coth\left(\frac{2J + 1}{2J} y\right) - \frac{1}{2J} \coth\left(\frac{y}{2J}\right), \quad (4)$$

$$y = \frac{J g_J \mu_B}{k_B T} H_m,$$

where  $J$  is the mean angular momentum and  $H_m$  is the molecular/crystal field.  $k_B$  is the Boltzmann constant. If the temperature  $T$  is lower than  $0.8T_C$ ,  $M_S(T) \approx M(T)$  [49]. The  $H_m$  is proportional to the exchange energy,  $H_m = A E_{exc}$ , or the atomic cohesive energy. Therefore, the  $T$  and  $K_j$  dependence of the  $M_S(K_j, T)$  can be obtained by replacing the  $J$  with the size dependent  $J(K_j)$  and  $E_{exc}(K_j)$  [44] that are given as:

$$E_{exc}(K_j) = E_{exc}(\infty) \left[ 1 + \sum_{i \leq 3} \gamma_{ij} (z_{ib} c_i^{-m} - 1) \right],$$

$$J(K_j) = J \left[ 1 + \sum_{i \leq 3} r_{ij} (c_i^{-m} - 1) \right], \quad (5)$$

$$\gamma_{ij} = \frac{\tau c_i}{K_j}.$$

The  $i$  is counted from the outermost atomic layer to the center of the solid up to three.  $\tau = 1, 2$  and  $3$  correspond to a plate, a rod, and a spherical dot. One needs to note that Eq. (5) does not apply to an isolated atom as no exchange interaction is involved.

## 3. MC simulation

### 3.1. Crystal structures

In order to examine the model consideration, MC simulation was carried out based on the BOLS incorporated Ising convention. The enhanced surface magnetic moment was taken into effect by varying the spin value  $S'_i$  for each atom. We employed six kinds of nanosolids in the MC simulation to investigate the effects of size, shape and structure on the  $M_S$  at various temperatures. They are fcc spherical dots, rods, and plates containing different number of atoms. Calculations were also conducted using the ordered structures of icosahedra, decahedra and the close-packed fcc truncated octahedra that are favored from the energetic point of view.

The fcc spherical dots are formed in such a way that layers of successive atoms are added to an atom in the center. Fig. 1(a) shows the fcc spherical dot containing  $N_{141}$  atoms with  $S = 9$  shells and  $K_j = 3.3$  radius. Here, we only consider those clusters with completely closed shells as a convention [36]. Table 1 lists the  $N_i$  values of the first 12 spherical particles. The rod system and the plate system are also formed based on the fcc lattice. The axis of the rod is chosen along the  $\langle 100 \rangle$  direction and the length is maintained at  $K_j = 28.3$ . The radius ranges from  $S = 1$  to  $11$  ( $K_j = 0.5-3.66$ ). The orientation

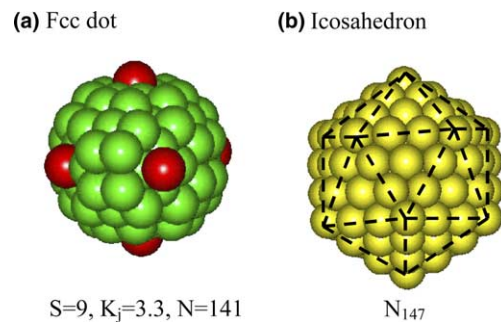


Fig. 1. Illustration of typical atomic configurations of: (a) fcc dot,  $S = 9$ ,  $K_j = 3.3$ ,  $N_{141}$  and (b) icosahedron  $N_{147}$ .

Table 1

Atomic distribution in the fcc spherical dot for Monte Carlo simulation ( $K_j$  is the layer number in unit of exchange bond length  $d$  and  $N_i$  is the atomic number of  $i$ th shell,  $N_j$  is the total number of atoms of the particle, and  $z_i$  is the CN of the atoms in the  $i$ th shell)

S (shell number)	$K_j$	$N_i$	$N_j = \sum N_i$	$z_i(N_j = 225)$
1	0.50	1	1	12
2	1.50	12	13	12
3	1.91	6	19	12
4	2.23	24	43	12
5	2.50	12	55	12
6	2.74	24	79	12
7	2.95	8	87	12
8	3.15	48	135	10
9	3.33	6	141	8
10	3.50	36	177	7
11	3.66	24	201	6
12	3.82	24	225	5

of the plate is also in the  $\langle 100 \rangle$  direction and the width and length are maintained at  $K_j = 28.3$ . The thickness ranges from  $S = 1$  to 14 ( $K_j = 0.5 \sim 5.1$ ). Fig. 1(b) shows the close-packed icosahedra with total number of  $N_{147}$  atoms, respectively. Icosahedra and decahedra are non-crystalline structures that cannot be found in bulk crystal because of their fivefold symmetry. Icosahedra are quasi-spherical, where atoms are arranged in concentric shells. Marks-truncated decahedra have reentrant  $(111)$  facets that are introduced via a modified-Wulff construction. An fcc truncated-octahedron owns the crystalline structure and has the open  $(100)$  facets. The numbers of atoms of the three kinds of particles are tabulated in Table 2.

### 3.2. MC algorithm

Initially, the lattice spins can be in hot or cool state. In a hot state, the spins orientate randomly; and in a cool state, the spins are aligned parallel to the applied magnetic field. In order to minimize the computational time, we employed in calculations cool state initialization when the temperature is low ( $k_B T/J_{\text{exc}} < 6$ ) and hot state initialization when the temperature is high ( $k_B T/J_{\text{exc}} \geq 6$ ).

Table 2

The number of atoms of the ordered and close-packed structures used in MC simulation

Icosahedron	Marks-decahedron	Fcc truncated-octahedron
$N_{13}$	$N_{75}$	$N_{19}^a$
$N_{55}$	$N_{101}$	$N_{38}$
$N_{147}$	$N_{318}^b$	$N_{79}$
$N_{309}$	$N_{389}^b$	$N_{201}$
		$N_{225}$
		$N_{260}$
		$N_{314}$
		$N_{405}$

<sup>a</sup> Decahedron.

<sup>b</sup> Fcc octahedron.

The value of the Hamiltonian  $H_{\text{prev}}$  for a specific spin system was calculated using Eq. (2). The spin  $S'_i$  was chosen randomly and the orientation was flipped from  $S'_i$  to  $S_{i,\text{trial}}$  and then the value of the Hamiltonian  $H_{\text{next}}$  was calculated again. The energy change for such a spin re-orientation is:

$$\Delta H = H_{\text{next}} - H_{\text{prev}}. \quad (6)$$

For simplicity, the Metropolis criterion was used to determine whether the new state is acceptable or not [50]. The energy change must satisfy the condition below for a successful spin orientation change:

$$e^{-\Delta H/k_B T} > r, \quad (7)$$

where  $r$  is a uniform random deviate. Sweeping every lattice site of the spin system gives out one MC step. Carried out several MC steps, the spin system will reach into a thermal equilibrium state for a specific size at a specific temperature.

## 4. Results and discussion

Fig. 2 shows the MC simulated  $M_S(K_j, T)$  curves at zero applied magnetic field for: (a) an fcc dot; (b) fcc rod; (c) fcc plate; (d) icosahedra spin systems. Generally, at very low  $T$  region ( $k_B T/J_{\text{exc}} < 3$ ), the  $M_S(K_j, T)$  increases with oscillatory features when the solid size is reduced. At mid- $T$  region ( $k_B T/J_{\text{exc}} \sim 6$ ), the  $M_S(K_j, T)$  drops monotonically with solid size. In the paramagnetic region, the residual  $M_S(K_j, T)$  increases as the size is reduced. These features are intrinsically common depending less on the shape and structure of a specific solid.

Fig. 3 shows the BOLS predicted  $M_S(K_j, T)$  counterplot for a spherical dot. No oscillatory features are given as we used a smooth function in Eq. (6) for the surface to volume ratio. The size induced  $M_S$  behavior at low temperature and at mid temperature is consistent with the MC simulation and the widely reported trends as well. One needs to note that Fig. 3 shows only the  $M_S$  behavior of particles with closed outermost atomic shells. Atoms in the incomplete outermost shells possess even higher  $M_S$  than those in the enclosed ones because of the large portion of lower-coordinated atoms.

### 4.1. Low- $T$ $M_S(K_j, T)$ enhancement

It is seen from Fig. 4(a) that for a specific size  $K_j$ , the  $M_S$  of the fcc dot is higher than that of the fcc plate because of the different dimensionality.<sup>19</sup> It is understood that when the temperature is very low,  $T \rightarrow 0$ ,  $y \rightarrow 8$ , and then  $B_J(y) \rightarrow 1$ , Eq. (5) can be approximated as:  $M_S(T \rightarrow 0) = Jg_j\mu_B$ . Using a shell structure in the BOLS correlation that calculates the magnetic moment of every atom layer-by-layer leads to the size-enhanced  $M_S$  for a nanosolid at very low temperature:

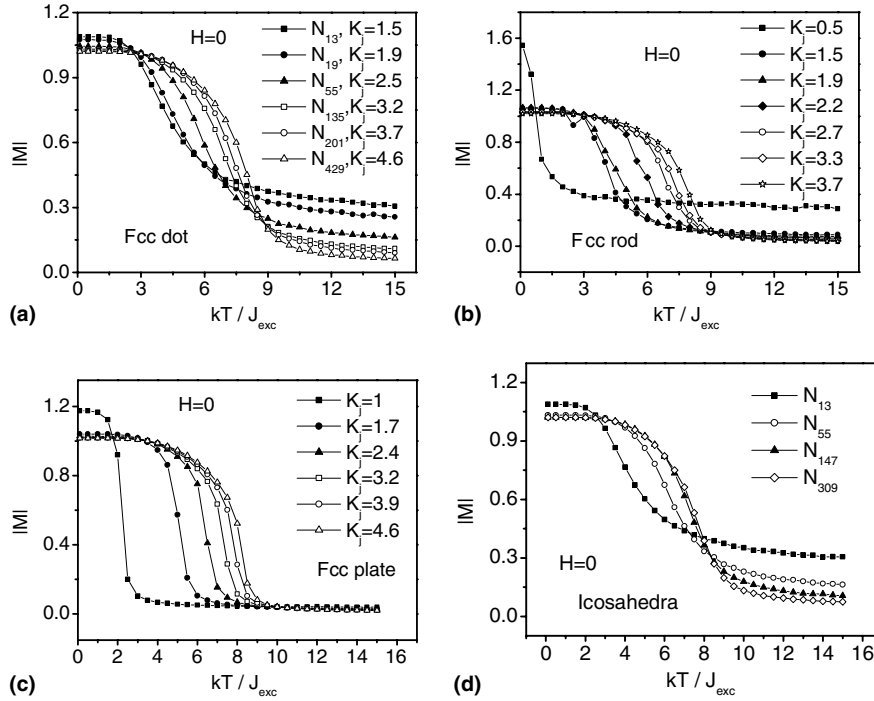


Fig. 2. MC simulation results on  $T$  and size dependence of the  $M_S$  for: (a) fcc dot; (b) fcc rod; (c) fcc plate; (d) icosahedron.

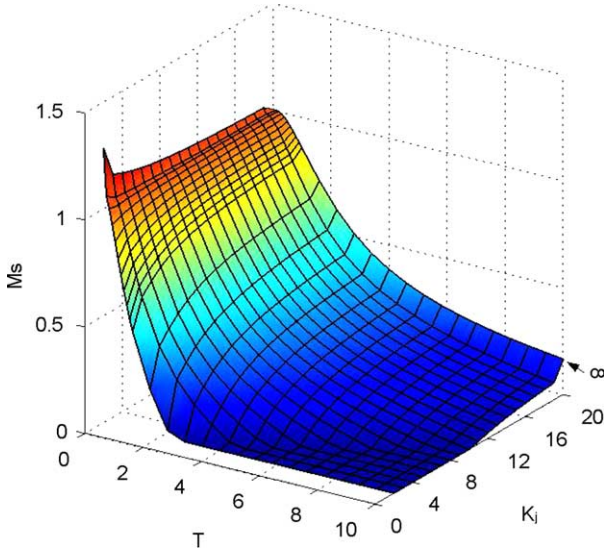


Fig. 3. BOLS-predicted  $M_S(K_j, T)$  counter plot shows that  $M_S$  increases with inverse size at low temperature and decreases with size at mid temperature. The  $M_S$  is normalized by  $M_S(T = 0, K_j = 8)$  and  $T$  is normalized by  $AE_{exc}$  (8).

$$\frac{\Delta M_S(K_j, T)}{M_S(\infty, T)} \Big|_{T \rightarrow 0} = \sum_{i \leq 3} r_{ij} (c_i^{-m} - 1). \quad (8)$$

Agreement of MC calculations and BOLS predictions as well as the observed trends confirm the validity of the BOLS consideration that the  $M_S$  enhancement is dominated by the strongly localized electrons in the surface skin.

#### 4.2. Mid- $T$ $M_S(K_j, T)$ suppression

Differentiating Eq. (5) against  $E_{exc}(K_j)$  leads to the  $M_S(K_j, T)$  in the mid  $T$  region:

$$\begin{aligned} \frac{\Delta M_S(K_j, T)}{M_S(\infty, T)} &= \frac{E_{exc}(\infty) N g_J^2 \mu_B^2 A}{2k_B T M_S(\infty, T)} \left\{ \csc h^2 \left[ \frac{g_J \mu_B}{k_B T} A E_{exc}(\infty) \right] \right. \\ &\quad \left. - (2J + 1)^2 \csc h^2 \left[ \frac{(2J + 1) g_J \mu_B}{2k_B T} A E_{exc}(\infty) \right] \right\} \frac{\Delta E_{exc}(K_j)}{E_{exc}(\infty)} \\ &= \alpha(J, T) \sum_{i \leq 3} \gamma_i (z_{ib} c_i^{-m} - 1), \end{aligned} \quad (9)$$

where parameter  $\alpha(J, T)$  is  $T$  and material dependent. At mid temperature, the size effect on the  $J$  becomes insignificant compared with the  $E_{exc}$ . Eq. (9) indicates that the tailoring of  $M_S$  at  $T$  closing to  $T_C$  is dominated by the  $E_{exc}$  that drops with solid size. At temperatures closing to  $T_C$ , thermal fluctuations of the spins are dominant. The drop of exchange energy determines the critical temperature of melting and phase transition [44]:

$$\frac{\Delta E_{exc}(K_j)}{E_{exc}(\infty)} = \frac{\Delta T_C(K_j)}{T_C(\infty)} = \frac{\Delta T_m(K_j)}{T_m(\infty)} = \sum_{i \leq 3} \gamma_{ij} (z_{ib} c_i^{-m} - 1). \quad (10)$$

Matching predictions based on Eq. (9) with  $\alpha(J, T) = 1.4$  to the MC simulative results are shown in Fig. 4(b). The calculated trend is consistent with the measurement as well.

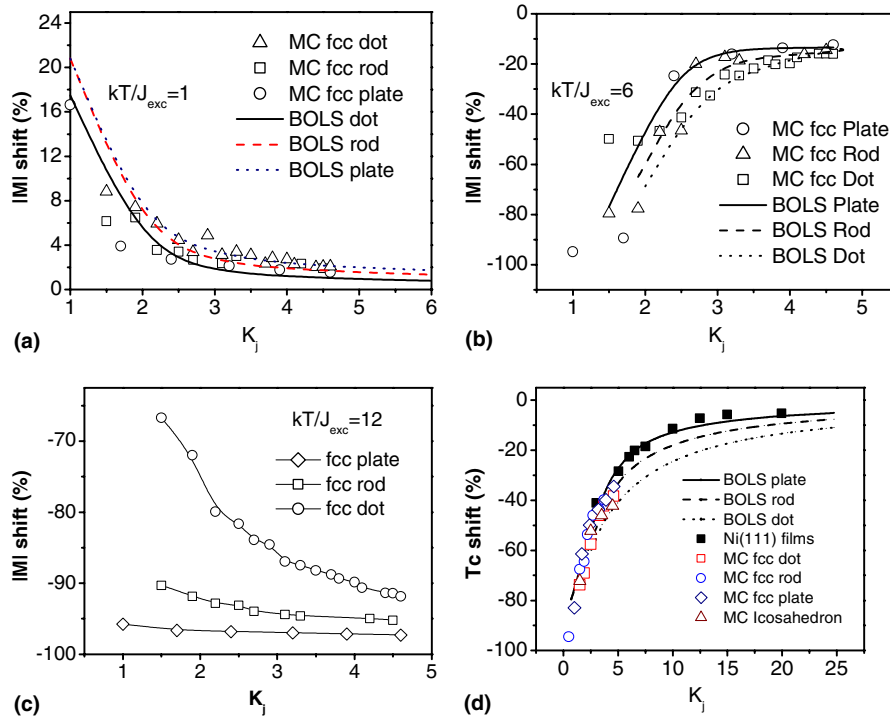


Fig. 4. Size dependence of the  $M_S$  at temperature  $k_B T/J_{exc}$ : (a) = 1; (b) = 6; (c) = 12, for fcc nanosolids shows three outstanding regions, where  $|M|$  shift =  $[|M|(K_j) - |M|(\infty)]/|M|(\infty) \times 100\%$ . (d) Comparison of the size-suppressed  $T_C$  derived from MC simulation, BOLS prediction, and measurements of Ni films [7].

In the paramagnetic phase as shown in Fig. 4(c), the remnant magnetism is higher for smaller particles, which has been attributed to the slower temperature decay in the Monte Carlo study and to the increasing fluctuations with decrease in cluster size [36].

Fig. 4(d) compares the  $T_C$  suppression as derived from MC and BOLS calculations and the experimentally observed  $T_C$  suppression of Ni/W films [7]. The  $d$  of nickel that is used in the normalization is 0.1244 nm and the  $T_C$  for bulk nickel is 631 K. Results show exceedingly well consistency between predictions and observations.

#### 4.3. $M_S(K_j, T \sim 0)$ oscillation and structural stability

Fig. 5 compares (a) the oscillation behavior of  $M_S$  of smaller clusters at low temperatures and (b) the surface-to-volume number ratio of the first surface layer of the fcc and bcc spherical dots. Agreement suggests that the oscillation originates from the surface-to-volume ratio because some particles may have fewer surface atoms with smaller  $\gamma_{ij}$  value than that of the adjacent larger or smaller ones. The oscillation behavior is consistent with observations made by Apse et al. [51] from Ni clusters of  $N_{13}$ ,  $N_{34}$  and  $N_{55-56}$  atoms at low temperatures. Therefore, it is reasonable to correlate the  $M_S$  oscillation to the surface-to-volume ratio with quantized features when one counts atom-by-atom.

The physical properties of a nanosolid in molecular regime typically exhibit a very irregular dependence on their aggregate size, namely, magic numbers, while they behave in a regular way in mesoscale. As can be seen, the icosahedron, Marks-decahedron and the fcc truncated-octahedron have lower  $M_S$  in the low- $T$  region and higher  $M_S$  in the mid- $T$  region, especially, the small icosahedral particles containing  $N_{55}$  and  $N_{147}$  atoms compared to other structures. In molecular regime, icosahedron has fewer low-CN atoms at the surface with most compact structure compared with other particles. The mass spectra of nanosolids usually exhibit especially abundant sizes that often reflect particularly stable structures, especially reactive nanosolids, or closed electronic shells [52]. These “magic number” sizes are of great theoretical interest since many of them correspond to compact structures that are especially stable. The magnetic moment of ferromagnetic nanosolid was reported to exhibit the same behavior [53]. The simulative results presented herewith show the same cases that  $N_{13}$ ,  $N_{55}$ ,  $N_{147}$  are the magic numbers for small magnetic nanoparticles, confirming icosahedron is the most closed structure when the size is small. However, when the size  $N_j$  is larger than 300, the fcc truncated-octahedron exhibits the smallest  $M_S$  in the low- $T$  region and the highest  $M_S$  in the mid- $T$  region, indicating that the fcc truncated-octahedron is the most compact structure when  $N_j > 300$  compared with decahedra, icosahedra

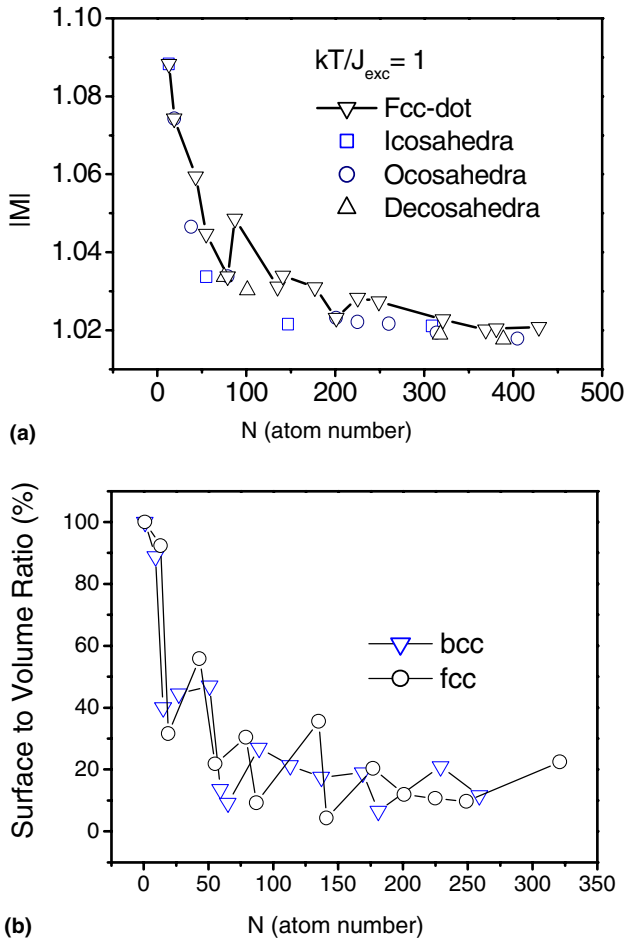


Fig. 5. Comparison of: (a) the MC derived  $M_S$  oscillations of at  $k_B T/J_{exc} = 1$  for various structures and (b) the quantized surface-to-volume number ratio of the first surface layer of fcc and bcc structures.

and fcc spherical dot. The MC simulation results here are consistent with a recent experimental work on copper particles, in which Reinhard [54] showed that the icosahedral structure dominates at sizes well below a diameter limit of 3.8 nm while the fcc particles occur close to this limit or above. The competition between the surface energy reduction and the strain energy enhancement determines the structural stability. Therefore, icosahedra are the most stable at small sizes due to its low surface energy and good quasispherical structures, while decahedra are favorable at intermediate sizes, and crystalline structures are recovered in the limit of large objects.

## 5. Conclusion

By incorporating the BOLS correlation to the Ising premise and the Brillouin equations, we have conducted the MC simulations and BOLS predictions to examine the size, shape, structure, and temperature dependence

of the magnetization of a ferromagnetic nanosolid. MC simulations and BOLS predictions have reproduced all the observed features including the  $M_S(K_j \sim 0, T \sim 0)$  oscillation with clear insight into the physics origin of the changes. It can be concluded as:

- (i) For a ferromagnetic nanosolid, the magnetic moment at very low temperature increases compared with the bulk value due to the densification and localization of surface charges that contribute to the angular momentum of the lower-coordinated atoms.
- (ii) The  $M_S$  at temperature around  $T_C$  reduces being dominated by the decrease of exchange energy that dictates the  $T_C$  suppression of the ferromagnetic system.
- (iii) The  $M_S$  oscillations with the total number of atoms arise from nothing more than the surface-to-volume ratio that depends on the shape and size of the nanosolid.
- (iv) When  $N_j < 300$ , the icosahedral particles exhibit the lowest  $M_S$  at low- $T$  and the highest  $M_S$  in the vicinity of  $T_C$ ; when  $N_j > 300$ , the fcc truncated-octahedron takes this trend in place. Therefore, icosahedral with less than 300 atoms is the most stable structure but the fcc truncated-octahedron with more than 300 atoms becomes most stable.
- (v) Consistency in the MC calculations, BOLS predictions, and experimental observations reconciles for the first time the discrepancy that some measured magnetic enhancement at low- $T$  and some measured magnetic tailoring at ambient temperatures and the  $M_S$  oscillates with size at low- $T$  for smaller sizes. Findings therefore evidence the tremendous impact of atomic CN imperfection to the physical behavior of a low dimensional system and the adequacy and reality of the BOLS correlation.

## References

- [1] Smyth JF, DiVincenzo DP, Smyth JF. *Science* 1992;258:414.
- [2] Ramirez AP. *J Phys: Condens Mat* 1997;9:8171.
- [3] Marchessault RH, Richard S, Rioux P. *Carbohydrate Res* 1992;224:133.
- [4] Hernando A, editor. *Nanomagnetism. Series E, vol. 247*. Dordrecht, Boston: Kluwer Academic; 1993.
- [5] Zhong WH, Sun CQ, Tay BK, Li S, Bai HL, Jiang EY. *J Phys: Condens Mat* 2002;14:L399.
- [6] Sun CQ, Zhong WH, Li S, Tay BK. *J Phys Chem B* 2004;108:1080.
- [7] Li Y, Baberschke K. *Phys Rev Lett* 1992;68:1208.
- [8] Tronc E, Noguès M, Chanéac C, Lucari F, D'Orazio F, Grenèche JM, et al. *J Magn Magn Mater* 2004;272–276:1474.
- [9] Seehra MS, Punnoose A. *Solid State Commun* 2003;128:299.
- [10] Zhong WH, Sun CQ, Li S. *Solid State Commun* 2004;130:603.
- [11] Heer WA, De Milani P, Chatelain A. *Phys Rev Lett* 1990;65:488.

- [12] Guzman M, Delplancke JL, Long CJ, Delwiche J, Hubin-Franskin MJ, Grandjean F. *J Appl Phys* 2002;92:2634.
- [13] Taniyama T, Ohta E, Sato T, Takeda M. *Phys Rev* 1997;B55:977.
- [14] Chinnasamy CN, Narayanasamy A, Ponpandian N, Chattopadhyay K, Saravanakumar M. *Mater Sci Eng* 2001;A304:408.
- [15] Qiang Y, Sabiryanov RF, Sjaswal S, Liu Y, Haberland H, Sellmyer DJ. *Phys Rev* 2002;B66:064404.
- [16] Falicov LM, Pierce DT, Bader SD, Gronsky R, Hathaway KB, Hopster HJ, et al. *J Mater Res* 1990;5:1299.
- [17] Aguilera-Granja F, Moran-Lepez JL. *Solid State Commun* 1990;74:155.
- [18] Geng WT, Freeman AJ, Wu RQ. *Phys Rev* 2001;B63:064427.
- [19] Cox DM, Trevor DJ, Whetten RL, Rohlfing EA, Kaldor A. *Phys Rev* 1985;B32:7290.
- [20] Bucher JP, Douglas DC, Xia P, Haynes B, Bloomfield LA. *Phys Rev Lett* 1991;66:3052.
- [21] Chen JP, Sorensen CM, Klabunde KJ, Hadjipanayis GC. *Phys Rev* 1995;B51:11527.
- [22] Ney A, Pouloupoulos P, Baberschke K. *Europhys Lett* 2001;54:820.
- [23] Konno M. *J Phys Soc Jpn* 1980;49:1185.
- [24] Liu F, Press MR, Khanna SN, Jena P. *Phys Rev* 1989;B39:6914.
- [25] Kodama RH, Berkowitz AE, McNiff Jr EJ, Foner S. *Phys Rev Lett* 1996;77:394.
- [26] Kodama RH, Berkowitz AE, McNiff Jr EJ, Foner S. *J Appl Phys* 1997;81:5552.
- [27] Sumiyama K, Sato T, Graham GM. *Solid State Commun* 1976;19:403.
- [28] Wedler G, Schneck H. *Thin Solid Films* 1977;47:147.
- [29] Ohta S, Terada A, Ishii Y, Hattori S. *Trans Inst Electron Commun Eng Jpn E* 1985;E68:173 [in English].
- [30] Crangel J. *Solid state magnetism*. New York: Van Nostrand Reinhold; 1991.
- [31] Mattis D. *Theory of magnetism*. Springer; 1985.
- [32] Rado G, Suhl H, editors. *Magnetism*. New York: Academic Press; 1963.
- [33] Merikoski J, Timonen J, Manninen M, Jena P. *Phys Rev Lett* 1991;66:938.
- [34] Huang ZG, Feng Q, Chen ZG, Chen SY, Du Y. *Microelectron Eng* 2003;66:128.
- [35] Han DH, Wang JP, Luo HL. *J Magn Mang Mater* 1994;136:176.
- [36] Merikoski J, Timonen J, Manninen M, Jena P. *Phys Rev Lett* 1991;66:938.
- [37] Jensen PJ, Bennemann KH. *Zeitschrift fur Physik* 1995;D35:273.
- [38] Pastor GM, Dorantes-Dvila J, Bennemann KH. *Chem Phys Lett* 1988;148:459.
- [39] Zhao J, Cben X, Sun Q, Liu E, Wang G. *Phys Lett* 1995;A205:308.
- [40] Aguilera-Granja F, Montejano-Carrizales JM, Morán-López JL. *Phys Lett* 1998;A242:255.
- [41] Kittel C. *Introduction to solid state physics*. 6th ed. New York: Wiley; 1986.
- [42] Kbanna SN, Linderoth S. *Phys Rev Lett* 1991;67:742.
- [43] Sun CQ. *Phys Rev* 2004;B69:045105.
- [44] Sun CQ, Wang Y, Tay BK, Li S, Huang H, Zhang Y. *J Phys Chem* 2002;B106:10701.
- [45] Sun CQ. *Prog Mater Sci* 2003;48:521.
- [46] Sun CQ, Bai HL, Li S, Tay BK, Jiang EY. *Acta Mater* 2004;52:501.
- [47] Sun CQ, Li S, Tay BK, Chen TP. *Acta Mater* 2002;50:4687.
- [48] Qian X, Hübner W. *Phys Rev* 1999;B60:16192.
- [49] Dai DS, Qian KS. *Ferromagnetism*. Beijing: Sci Press; 2000.
- [50] Metropolis N, Rosenbluth A, Rosenbluth M, Teller A, Teller E. *J Chem Phys* 1953;21:1087.
- [51] Apsel SE, Emmert JW, Deng J, Bloomfield LA. *Phys Rev Lett* 1996;76:1441.
- [52] Sakurai M, Watanabe K, Sumiyama K, Suzuki K. *J Chem Phys* 1999;111:235.
- [53] Yang CY, Johnson KH, Salahub DR, Kaspar J, Messmer RP. *Phys Rev* 1981;B24:5673.
- [54] Reinhard D. *Phys Rev Lett* 1997;79:1459.